aerospace

MDPI

Article

Methods for Analyzing Avionics Reliability Reflecting Atmospheric Radiation in the Preliminary Development Phase: An Integrated Failure Rate Analysis

Dongmin Lee [1] and Jongwhoa Na [2,*]

[1] School of Smart Air Mobility, Korea Aerospace University, Goyang-si 10540, Republic of Korea; leedongmin93@kau.kr
[2] School of Electronics and Information Engineering, Korea Aerospace University, 76 Hanggongdaehang-ro, Deogyang-gu, Goyang-si 10540, Republic of Korea
* Correspondence: jwna@kau.ac.kr; Tel.: +82-2-300-0410

Abstract: Advances in deep submicron semiconductor technology have increased the significance of studying soft errors caused by atmospheric radiation in avionics systems. Atmospheric radiation particles, such as protons and neutrons, can induce Single Event Upsets (SEUs) in sensitive electronic components, leading to system malfunctions and data corruption. Traditional reliability analysis based on older IC or LSI components may fail to account for radiation-induced effects. However, modern avionics systems equipped with state-of-the-art VLSI components are increasingly susceptible to Single Event Upsets (SEUs), potentially leading to underestimated failure rates in these advanced systems. This study introduces an integrated failure rate analysis that incorporates both the physics of failure rates resulting from aging and wear-out and soft error rates induced by atmospheric radiation. The proposed failure rate analysis of the reliability of avionics operating at altitudes of up to 18 km by combining the physics of failure rates with radiation-induced failure rates was derived using a semi-empirical SEU estimation method. Case studies using the Zynq 7000 board, sourced from AMD (San Jose, USA), confirmed that the integrated failure rate analysis provides more accurate reliability predictions compared to conventional analysis. This approach is expected to improve the accuracy of safety assessments during the preliminary development stages, leading to a shortened development timeline and enhanced design quality.

Keywords: avionics; atmospheric radiation; soft error rate; physics of failure; reliability

Academic Editors: Davide Ferretto and Fabrizio Stesina

Received: 31 December 2024
Revised: 28 January 2025
Accepted: 29 January 2025
Published: 3 February 2025

Citation: Lee, D.; Na, J. Methods for Analyzing Avionics Reliability Reflecting Atmospheric Radiation in the Preliminary Development Phase: An Integrated Failure Rate Analysis. *Aerospace* **2025**, *12*, 118. https://doi.org/10.3390/aerospace12020118

1. Introduction

Advances in deep submicron semiconductor technology have increased the significance of studying soft errors caused by atmospheric radiation in avionics systems [1–5]. Atmospheric radiation, also called secondary cosmic radiation, consists of particles (protons, neutrons, muons, etc.) that penetrate the Earth's magnetic field, reach the atmosphere, and interact with the internal structure of the VLSI components. This can result in a Single Event Upset (SEU) in data storage devices such as memory, flip-flops, and latches [1]. An SEU in memory or an SET in a logic circuit can propagate once latched, potentially leading to system errors. This propagation may result in unintended bit flips and subsequent system malfunctions. Recent studies have shown that as semiconductor processes become more miniaturized, the risk of SEUs increases [2]. As VLSI technology continues

to scale down to the nanoscale, the impact of atmospheric radiation becomes increasingly significant.

Traditional reliability analysis of avionics boards predominantly relies on failure rate data associated with aging derived from component manufacturing processes and operational environment conditions. Typical hardware reliability analyses for electronic equipment use MIL-HDBK-217, etc. [6–8]. These techniques do not accurately reflect the actual operating environment due to the lack of sufficient field failure rates and rapidly developing VLSI technologies [9]. To improve the accuracy of aging-related failure rate data, the physics of failure (PoF) analysis are introduced [10,11]. PoF analysis involves digital modeling of the target system by considering component elements and analyzing it by incorporating operating environment parameters. Compared to conventional reliability analysis methods, PoF analysis can provide a more detailed analysis of electronic equipment.

In addition to aging-related failure rates, the reliability analysis of modern avionics systems equipped with state-of-the-art VLSI components must account for the radiation-induced failure rates caused by atmospheric radiation. This radiation is known to induce transient faults, which can significantly impact the performance and reliability of nanoscale VLSI components in modern avionics systems [12,13].

Atmospheric radiation primarily causes failures such as bit flipping in memory. This atmospheric radiation increases with altitude, peaking at its highest levels around 18 km [14–16]. At subsonic flight altitudes (12 km), particle fluxes are approximately 300 times greater than at sea level, and at 18 km, they are 500 times higher [14]. Considering that avionics consist of large numbers of memory-based devices, these radiation events cannot be ignored [15,16]. Currently, the reliability of avionics at high operational altitudes is relatively underestimated, which negatively impacts both aircraft maintenance and safety.

The goal of this study is to develop an integrated failure rate (IFR) analysis combining aging-related failures with soft error rates induced by atmospheric radiation. The IFR analysis is defined as the sum of two components: a physics of failure-based aging-related failure rate that incorporates environmental stressors and a soft error rate that captures the failure rate due to radiation effects from atmospheric particles. To calculate the aging-related failure rate, the model integrates component information of the target electronic system board along with key operating environment parameters such as temperature and operational time. This calculation is based on a physics of failure methodology that reflects the physical degradation processes occurring in the system. Meanwhile, the radiation-induced failure rate is determined using a semi-empirical soft error rate (SER) estimation approach, which estimates the system failure rate resulting from Single Event Upsets (SEUs) caused by atmospheric radiation [17]. In this study, statistical fault injection simulations were conducted to quantify system failures arising from soft errors.

The proposed IFR analysis method has the following advantages: (1) It can reduce hardware design costs by allowing the use of the commercial FPGA board based on hardware IP and mission time during the preliminary development phase. (2) It improves accuracy by comprehensively evaluating various factors affecting the reliability of electronic components. As a result, the proposed integrated failure rate analysis method enables system safety analysis with improved accuracy during the preliminary development phase. In the development of avionics systems, where effectively managing costs and timelines is crucial, our approach may help optimize system development expenses while enhancing safety and reliability.

A case study was conducted to validate the proposed IFR analysis, and the results confirmed that it provides more accurate failure rate estimations compared to existing estimation methods. Twenty-three benchmark hardware IPs at various levels were

selected targeting the Zynq 7000 board, and their aging failure rate and radiation failure rates were calculated. For the calculation of the aging failure rate, the PoF analysis was conducted based on the temperature profile prepared according to MIL-STD-810H after modeling the target board [18]. For the calculation of the radiation failure rate, a statistical fault injection test was performed using the Verilog Fault Injector tool, and a semi-empirical SER estimation model was applied. The failure rates of two Circuit Card Assemblies from Northrop Grumman's MODAR program were compared with the failure rate estimated using the IFR method [6]. The results showed an error margin of less than 1% at 13,000 h of operation, confirming the accuracy and validity of the IFR analysis.

The remainder of this document is organized as follows: Section 2 discusses the current failure rate analysis methods and raises questions regarding their effectiveness. Section 3 introduces the concept of the integrated failure rate and explains how it can be calculated. Section 4 analyzes the integrated failure rate for various benchmark circuits and compares the previous failure rate analysis with field data. Finally, Section 5 concludes the paper.

2. Background

Section 2 discusses the impact of space atmospheric radiation on the reliability of electronic equipment, as well as various methodologies for analyzing this phenomenon and the limitations of existing reliability assessment approaches. Section 2.1 explains the causes of space atmospheric radiation and how this radiation affects the reliability of electronic equipment. Section 2.2 introduces methods for analyzing the reliability of electronic equipment in relation to space radiation, discussing the advantages and disadvantages of each method. Section 2.3 reviews existing reliability methodologies for electronic equipment and explains the limitations of these approaches in adequately accounting for space atmospheric radiation.

2.1. Atmospheric Radiation Effects on Avionics

As semiconductor process technology becomes more sophisticated, the number of defects caused by soft errors is increasing [13,19]. In particular, single event upsets (SEUs) in memory or SETs in logic circuits, which may propagate and cause system errors if latched, can result in unintended bit flips and system malfunctions. These phenomena occur mainly when high-energy ionized particles, such as cosmic rays, collide with the semiconductor structures of electronic devices, including field programmable gate arrays (FPGAs). These cosmic rays are emitted directly from the outer environment of space, including primary cosmic rays (PCR) and secondary cosmic rays (SCR), which are generated as primary cosmic rays enter the Earth's atmosphere. In this study, we focus exclusively on secondary cosmic rays.

Secondary cosmic rays consist of approximately three particles per cm^2s and are produced by collisions with air atoms such as nitrogen and oxygen when primary cosmic rays enter the Earth's atmosphere [20]. These secondary cosmic rays initially exist in small numbers, but their quantity increases as they interact with more atoms and undergo a multi-step particle process. Most of the charged particles produced recombine, and neutral particles, such as neutrons, lose energy as they travel through the atmosphere toward the Earth, eventually being mostly absorbed. However, some neutrons reach the ground, which is a major contributor to single event upsets (SEUs) in electronic devices. In other words, the soft errors that occur in the geosphere are effects of secondary cosmic rays.

Failures of electronic equipment exposed to cosmic atmospheric radiation are classified into two types: Total Ionizing Dose (TID) and Single Event Effect (SEE) failures [21,22]. Regular replacement intervals can prevent serious failures caused by TIDs. However, soft errors caused by SEEs are random and temporary, so they cannot be resolved by

replacement cycles alone. Therefore, it is important to assess the impact of these failures in advance. To achieve this, the soft error rate (SER) is used as a representative indicator to assess the probability of a soft error occurring per hour [23].

2.2. Trends and Advances in Radiation-Induced Failure Rate Analysis

The most direct and traditional method for measuring the Soft Error Rate (SER) is radiation testing [24–28]. Radiation testing evaluates the SER of a substrate by emitting various particles using a particle accelerator to simulate the actual conditions of the target substrate. These testing methods can be broadly categorized into two groups:

The first group consists of particle beam-based tests, which use high-energy particles such as heavy ions, protons, and neutrons to assess soft errors [24–26]. Heavy ion beam testing allows for precise SER analysis by emitting small particles; however, the high costs associated with the specialized facilities required for ion generation are a significant drawback [25]. Proton and neutron beam tests are also utilized for SER evaluation tailored to their respective environments, effectively simulating both space radiation and terrestrial conditions through the use of various particle types [5,26].

The second group comprises laser-based tests, which inject defects by generating electron–hole pairs within semiconductors using lasers [27,28]. Laser-based methods offer the advantages of relatively lower equipment costs and the ability to precisely inject defects at specific locations. However, due to the larger particle size, their precision may be inferior compared to particle beam-based tests. These hardware defect injection methods provide common benefits such as short processing times, low complexity, and accurate SER evaluation from a system perspective. Nevertheless, they also present specific challenges, including evaluation costs, reproducibility of test results, and defect propagation analysis.

Various software simulation approaches have been investigated to mitigate the high costs associated with cosmic radiation testing [29–36]. These approaches utilize simulation-based fault injection platforms to analyze the soft error rate (SER) of circuits. Simulation methods are broadly categorized into (1) static approaches and (2) dynamic approaches.

1. Static approaches analyze SER using semiotic methods and algebraic or probabilistic techniques based on specific data structures [29–32].
2. Dynamic approaches inject faults into the circuit and then perform simulations to analyze SER [33–36].

This simulation analysis method is less expensive than radiation testing and provides more accurate sensitivity analysis because it can assess both SER and injection sites. However, as the complexity of the analyzed circuit increases, the simulation time becomes longer, and the difficulty of the analysis also increases.

This study utilizes a kernel-based fault injection technique and a soft error rate (SER) estimation method employing a semi-empirical model. Existing simulation methods prioritize the accuracy of SER estimation results, which necessitates numerous parameters and complex calculation processes, thereby making them difficult to apply. Consequently, SER analysis of complex and critical circuits in aerospace is not only challenging but also impractical due to computational time constraints. The SER estimation technique presented in this study is based on existing radiation information (Single Event Upset) and employs a kernel-based fault injection technique using the Architectural Vulnerability Factor (AVF). This approach allows for the rapid and straightforward estimation of the circuit's approximate SER from the design stage. These features are summarized in Table 1.

Table 1. Comparison of radiation failure rate methods [24–36].

Methods	Test Duration	Number of Test Devices	Test Cost	Complexity	Accessibility
Radiation Test	Low	High	High	Low	Low
Software Simulation	High	Low	Middle	High	Middle
Semi-Empirical Methods	Middle	Low	Low	Middle	High

2.3. Electronic Equipment Reliability Analysis Methods and Limitations

MIL-HDBK-217 was first introduced in 1961 and has been widely used as a standard for predicting the reliability of electronic components and systems [8]. This handbook provides failure rate models for components such as integrated circuits, transistors, and capacitors. Initially focused on military and aerospace applications, its usage later expanded across various industries. However, since the 1980s, questions have been raised regarding the applicability and accuracy of MIL-HDBK-217 [10,37].

One of the key issues is the modeling approach that assumes a constant failure rate. Such an approach fails to capture the dynamic nature of actual electronic component failure rates, which change over time. Aishwarya Gaonkar et al. emphasize that modern electronic components generally begin to experience wear-out failure mechanisms early in their lifecycle, and a constant failure rate assumption does not adequately explain this behavior [38]. Additionally, Michael Pech and Wen-Chang Kang have pointed out that by neglecting factors such as design complexity, thermal interactions, and environmental influences on reliability, the handbook's results can diverge significantly from actual data [39].

IEEE Standard 1413.1 proposes a more sophisticated approach to address these issues [37]. This standard aims to overcome the limitations of MIL-HDBK-217 by reflecting multiple failure mechanisms and emphasizing modeling based on real environmental data. Moreover, Georgia-Ann Klutke et al. have indicated that the bathtub curve model is unsuitable for describing the failure rate trends of electronic systems, pointing out that the misinterpretation of historical data has led to inaccurate use of constant failure rate models [40].

In conclusion, while MIL-HDBK-217 was a useful tool in its early days, it has limitations in reflecting the dynamic and complex characteristics of modern electronic components and systems. Consequently, recent research and standards are moving toward integrating physical failure mechanisms and experimental data to provide more accurate reliability predictions [41].

To overcome these limitations, the physics of failure (PoF) has emerged as a core approach in modern reliability design [42,43]. PoF is a reliability design methodology that investigates the failure mechanisms of components under appropriate conditions throughout their lifecycle. Such failure mechanisms typically arise from stresses or wear due to material selection, mechanical stress, electrical stress, thermal effects, and chemical interactions. While traditional MIL-HDBK-217 methodologies do not consider wear-out mechanisms, PoF supports modeling by using information such as component specifications and operating environments. Recent studies suggest that using calibrated prediction tools together with PoF models enables intelligent asset management, thereby improving availability and safety [10].

To support the reliability analysis techniques, various reliability analysis tools have been developed. These reliability models estimate the failure rate of integrated circuits (ICs) by collecting information on device components, environmental factors, or empirical data. However, these tools do not consider the internal characteristics of the device's hardware intellectual property (HW IP) or the effects of space radiation [11,12]. This omission

can lead to significant errors in reliability prediction for highly reliable electronic warfare systems. Therefore, it is essential to develop new modeling approaches that can effectively evaluate the reliability of systems operating at high altitudes.

3. Reliability Analysis Method for Electronic Equipment Considering Atmospheric Radiation

Section 3 describes an integrated failure rate analysis for evaluating the reliability of electronic equipment that accounts for atmospheric radiation from the early development stages. This analysis incorporates both internal factors, such as wear-out mechanisms, and external factors, such as space atmospheric radiation, to calculate the reliability of electronic equipment. These procedures can be summarized as shown in Figure 1. Section 3.1 explains the integrated failure rate. Section 3.2 details a physics of failure (PoF) analysis method that leverages component information and operational environment data to reflect wear-out factors over time. Section 3.3 introduces a semi-empirical SER analysis method that employs statistical-based fault injection techniques to estimate system failure rates due to atmospheric radiation.

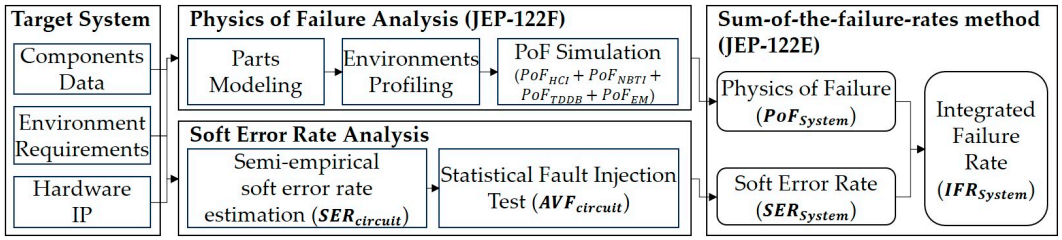

Figure 1. Integrated failure rate analysis framework combining physics of failure and soft error rate methodologies.

3.1. Integrated Failure Rate

Using the sum-of-the-failure-rates method, we describe the integrated failure rate that combines the physics of failure (PoF) corresponding to the aging failure rate and the soft error rate due to space atmosphere radiation. The integrated failure rate (IFR_{System}) is defined as the sum of the physics of failure rate (PoF_{System}) derived from the physics of failure (PoF) analysis and the soft error rate (SER_{System}) obtained through the statistical fault injection test, as shown in Equation (1):

$$IFR_{System} = PoF_{System} + SER_{System} \quad (1)$$

The physics of failure rates and soft error rates originate from distinct failure mechanisms and can be considered independent. In the document "Failure Mechanisms and Models for Semiconductor Devices" (JEP-122F), it is noted that PoF models do not incorporate radiation-related parameters [44]. Furthermore, the NASA PoF Handbook states that PoF model equations do not include radiation parameters and that radiation-induced failures should be treated separately from wear-out and degradation [42]. Therefore, by applying the Sum-of-the-Failure-Rates Method as outlined in JEDEC JEP122E, the integrated failure rate can be calculated by summing the physics of failure rate and soft error rate [44,45].

While this study analyzed PoF and SER independently, there is an opportunity to further explore how the aging of electronic components and the degradation of their physical properties might influence radiation-induced failures. Understanding these in-tractions could enhance the reliability assessments of devices operating in radiation-prone environments over extended periods. Future research may consider developing more

integrated reliability models that account for the interplay between aging, wear-out mechanisms, and radiation sensitivity.

3.2. Reliability Analysis Using Physics of Failure Rate Analysis

3.2.1. Physics of Failure

To predict product life using failure physics, we utilized Ansys' Sherlock software (2024 R2). Sherlock software can predict the lifespan of a product by performing semiconductor wear-out analysis on benchmark circuits. To conduct semiconductor wear-out analysis, information on semiconductor materials, property sizes, electrical properties, and operating conditions is required. Sherlock software estimates the system's lifetime based on four failure models presented in JEP-122F: hot carrier injection, negative bias temperature instability, time-dependent dielectric breakdown, and electromigration [44]. We can calculate the failure rate of the system through four PoF analyses, as shown in Equation (2).

$$PoF_{System} = PoF_{HCI} + PoF_{NBTI} + PoF_{TDDB} + PoF_{EM} \quad (2)$$

Hot Carrier Injection (HCI, PoF_{HCI}): This phenomenon occurs when the threshold voltage of a transistor increases and the current decreases due to the presence of hot carriers. The likelihood of HCI/HCE increases with longer transistor lifespans or smaller transistor sizes. The mathematical formulation for PoF_{HCI} is presented as Equation (A1) in Appendix A.

Negative Bias Temperature Instability (NBTI, PoF_{NBTI}): When a device operates at high temperatures with a negative voltage applied to the gate, the device's characteristics become unstable. Bias Temperature Instability is categorized into Positive Bias Temperature Instability (PBTI) occurring in NMOS transistors and Negative Bias Temperature Instability (NBTI) occurring in PMOS transistors. Notably, NBTI is more severe than PBTI and is therefore a primary focus in reliability analyses. A mathematical representation of PoF_{NBTI} is included in Equation (A2) in Appendix A.

Time-Dependent Dielectric Breakdown (TDDB, PoF_{TDDB}): This phenomenon involves the deterioration and eventual breakdown of the oxide film during prolonged operation at low voltage. TDDB (Time-Dependent Dielectric Breakdown) can be divided into three distinct phases based on the time of occurrence. The Initial Failure Phase involves the destruction of the oxide film caused by pinholes. Next, the Accidental Failure Phase occurs, where destruction happens at weak points within the oxide film, such as voids. Finally, the Wear Failure Phase represents a gradual destruction that progresses based on the inherent characteristics of the material. The mathematical equations for PoF_{TDDB} are provided in Equation (A3) in Appendix A.

Electromigration (EM, PoF_{EM}): EM is the movement of metal atoms caused by the transfer of momentum between electrons and metal nuclei. This movement can result in voids, which may lead to open circuits, or hillocks, which can cause short circuits between wiring lines. The equation for PoF_{EM} is elaborated in Equation (A4).

Understanding and analyzing these failure mechanisms is essential for predicting product life and enhancing reliability. By comprehensively considering the impact and probability of each failure mode, the durability of a product can be strengthened from the design stage. This approach enables the early prediction of semiconductor device degradation and the implementation of design improvements to minimize the likelihood of failure. Ultimately, an approach based on physics of failure contributes to increasing product reliability while reducing the costs associated with unplanned failures.

3.2.2. Physics of Failure Analysis Simulation

To analyze the physics of failure rate, we utilized Ansys Sherlock software to perform a PoF analysis on the IC chip of the target board component. The process comprised three main steps: environment and configuration setup, simulation, and PoF analysis.

First, during the environment and configuration setup phase, the components and operating environment of the target system were modeled. Using the acquired IC data, a detailed component model was constructed in Sherlock by inputting information such as the package type, lead details, fabrication materials, electrical and thermal characteristics, and test acceleration factors. External environmental conditions, defined by standards like MIL-STD-810H, were incorporated, particularly temperature profiles, as shown in Figure 2. This step simulated the environmental conditions the IC might encounter, forming a foundation for lifetime prediction and durability analysis.

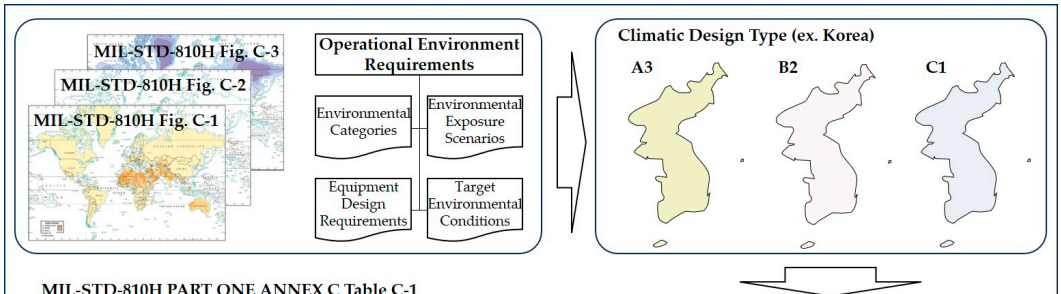

MIL-STD-810H PART ONE ANNEX C Table C-1

Climatic Design Type	Ambient Air Temperature (°C)	Solar Radiation (W/m²)	Ambient Relative Humidity (%RH)	Storage & Transit Temperature (°C)	Induced Relative Humidity (%RH)
A3 (Intermediate)	28 (Low), 39 (High)	0 to 1030	78 to 43	28 (Low), 82 (High)	See note*
B2 (Variable High Humidity)	26 (Low), 35 (High)	0 to 970	100 to 74	30 (Low), 63 (High)	75 to 19
C1 (Basic Cold)	−32 (Low), −21 (High)	Negligible	Tending toward saturation	−33 (Low), −28 (High)	Tending toward saturation

**Relative humidity for the A3 storage condition vary to widely between different situations to be represented by a single set of conditions.*

Figure 2. Electronic equipment operation and non-operating environmental temperature table by environmental category (MIL-STD-810H) [18].

Second, during the simulation stage, wear-out analysis of the IC was conducted using the configured component model and temperature profile. External IC information and predefined environmental conditions were used. The simulation output generated four physics of failure rate values, which were aggregated to produce a graph depicting the failure probability over time, as shown in Figure 3.

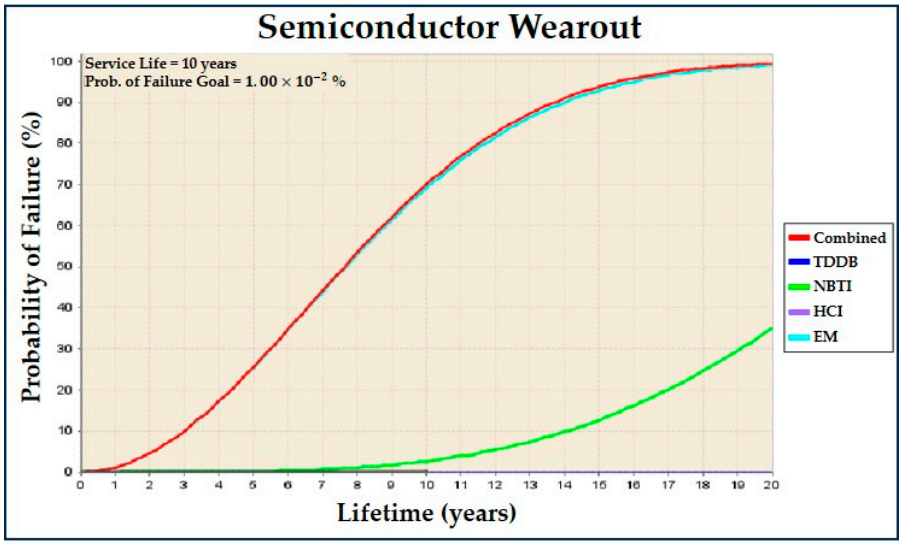

Figure 3. Physics of failure graph.

Third, in the PoF analysis step, Sherlock software was used to estimate physical failure rates based on the modeled components and temperature profiles. A detailed description of these procedures is provided in Section 4.2.

3.3. Radiation Failure Rate Analysis

3.3.1. Semi-Empirical Soft Error Rate Estimation

To obtain the integrated failure rate for the safety assessment at the preliminary design stage, it is necessary to include the radiation failure rate due to the particle interactions in the atmospheric environment. In the preliminary development phase, the budget and the schedule for the radiation test may be limited. In this case, we may need a fast and cost-effective method to estimate the radiation failure rate that can be used to select the optimal fault tolerant avionics architecture. It is important to note that we have four types of fault-tolerant mechanisms (FTMs), which are the hardware, software, information, and temporal redundancies, and each type has hundreds of unique-fault tolerant mechanisms [46,47]. The semi-empirical SER estimation model has the advantage of calculating the atmospheric radiation failure rate using prior failure rate information and statistical fault injection campaign at the preliminary development phase [17]. At the system level, the integrated failure rate (SER_{System}) is presented as follows:

$$SER_{System} = AVF_{circuit} \times Area \times SER_{circuit} \quad (3)$$

The Architectural Vulnerability Factor ($AVF_{circuit}$) quantifies the likelihood that a hardware fault will manifest as a software-visible error in a computing system. The $AVF_{circuit}$ is measured through statistical fault injection simulations. Bits are classified during fault injection testing into those that cause failures, known as ACE (Active Critical Errors) bits, and those that are masked, known as unACE bits. The $AVF_{circuit}$ is calculated as the ratio of ACE bits to the total number of bits in the circuit.

The $Area$ refers to the physical area of the actual circuit or system that is affected in the soft error rate calculation. This area is a key factor in determining the likelihood of exposure to external influences such as collisions with radiation particles or neutrons.

The $SER_{circuit}$ denotes the hourly probability of a soft error occurring within the system's circuit. In order to calculate $SER_{circuit}$ the atmospheric radiation failure rate at the circuit level, radiation acceleration test and circuit simulation data are required, as shown in Equation (4). Here, $\Phi_{radiation}$ represents the flux of radiation particles incident on the circuit, and $\sigma_{circuit}$ denotes the cross-sectional area where bit flips occur within the circuit.

$$SER_{Circuit} \cong \Phi_{radiation} \times \sigma_{circuit} \quad (4)$$

To obtain $\Phi_{radiation}$, it is necessary to investigate the neutron flux and energy spectrum for each region of the system. Cosmic radiation particles are produced in the sun and reach Earth, where they decrease as they collide with the Earth's magnetic field and atmosphere. The neutron flux and energy spectra are measured using extended energy spectroscopy [23,24]. The intensity of cosmic ray-induced neutrons in the atmosphere varies with altitude, geomagnetic field position, and solar activity [48,49]. Therefore, in order to calculate the radiation failure rate, the effect of neutron flux must be examined, taking into account the operating area of the system (latitude/longitude), altitude, and time of operation (solar activity). The flux calculator supports the calculation of relative flux compatible with the JEDEC standard JESD89 [50] and calculates the radiation failure rate by considering the latitude, longitude, altitude, and solar modulation parameters of the system's operating location. Latitude is measured relative to the equator, with northern positions entered as positive values and southern positions as negative values. Longitude is based on the prime meridian, with western positions entered as positive values and

eastern positions as negative values. For altitude, either the height above sea level or the atmospheric pressure can be entered. The solar modulation parameter accounts for the effect of sunspot activity on neutron flux. For most calculations, this effect is less than 10% of the total flux, and a default value of 50% is sufficient. This parameter can be adjusted by entering a value between 0 and 100 to represent the modulation ratio.

By employing a hardware fault injection approach, $\sigma_{circuit}$ can be verified. The estimate of the cross-section depends on the type of radiation particles emitted in the circuit and the amount of energy emitted in the circuit, in addition to the circuit characteristics such as the process of the semiconductor and the driving voltage/current/speed. To determine the estimate of the cross-section of the circuit, a test to reproduce the radiation environment in space is necessary. The artificial space radiation environment reproduction facility uses a proton accelerator to radiate heavy ions into the target circuit to measure SEU. The estimate of the cross-section of the test circuit is calculated by obtaining the number of SEU occurrences compared to the total number of fluences emitted on the test board. The $\sigma_{circuit}$ collects and analyzes the estimates of cross-section data published by research institutes. As a representative example, radiation testing results on a microcontroller conducted at TRIUMF, a Canadian particle accelerator facility, can be utilized for this purpose [5].

3.3.2. Statistical Fault Injection Simulation

To calculate $AVF_{circuit}$, a statistical defect injection test based on a dynamic model was conducted. Dynamic model-based analysis methods inject defects into a viable model, collect and analyze the results, and statistically calculate the failure rate. Dynamic model-based vulnerability analysis methods include (1) simulation-based fault injection and (2) emulation-based fault injection. Simulation-based fault injection methods perform Monte-Carlo Fault Injection (MCFI) on the simulated model to calculate a statistically significant derating rate $AVF_{circuit}$ [51,52]. The advantage of simulation techniques is that the test method is simple and can be utilized in the early stages of system development. However, they often consume a lot of time due to the need for repeated simulations. Dynamic model-based analysis methods use an operational model or circuit for analysis, allowing the characteristics of the digital circuit's usage to be reflected in the test results. Additionally, vulnerability factor analysis can be conducted concurrently with development. However, conducting a large number of tests to obtain results requires a high-performance defect injection testing environment to support the process for $AVF_{circuit}$ analysis.

For the purpose of analyzing the vulnerability factors of the hardware design model, the Verilog Fault Injector (VFI) environment was used [48]. The VFI environment is a fault injection testing tool developed based on the Verilog procedure interface (VPI). VFI is an interface function defined in IEEE 1364-2001 that allows you to link a custom model with a simulator [53]. Using VPI, you can view and change the internal state (signal, port, and reg) of the model being simulated. It is also possible to connect to heterogeneous simulators or external equipment. Most Verilog simulators support VPI functions, which ensures the portability of VFI environments.

Using the VFI test environment, faults are injected, and four types of failures are classified accordingly. The VFI test environment injects fault values such as transient stuck-at-0 and transient stuck-at-1. Depending on the defect injection value and the injection time and location, the defect value may match the logical value of the fault injection location. Once the defect is masked, the fault injection simulation behaves the same as the golden run. The results of the defect injection simulation are classified into the following four categories.

1) Benign Fault: The injected fault has not had any effect on the system. This is the case when the defect is applied and the changed value is the same as the normal value. Therefore, the fault injection run VCD has the same pattern as the golden run VCD.

2) Masking Fault: A fault that is temporarily present in the system but has no lasting impact, as it is masked by various factors. Masking can occur due to clock timing windows, logical or architectural conditions, or software-level factors.

3) Silent data corruption (SDC): A system failure occurs without detecting a defect. SDC is very dangerous because it is a failure state that occurs and yet remains undetected by the system. In order for the system to detect the occurrence of a fault, it must have a built-in fault detection unit. Any failure of a system that does not have a built-in fault detection unit is classified as SDC. In systems with built-in fault detection units, SDC can be used as a measure to evaluate fault detection performance.

4) Detected Unrecoverable Error (DUE): The DUE occurs when a fault detection mechanism identifies a defect but is unable to recover from it. For instance, consider a memory system equipped with Error-Correcting Code (ECC) that can detect two-bit errors and correct one-bit errors. In this system, if a two-bit error occurs, the error will be detected but cannot be corrected, leading to a Detected Unrecoverable Error (DUE). In such cases, although the system can identify the presence of an error, it fails to accurately restore the original data or state. In many cases, DUEs can lead to application or system crashes, hangs, or even necessitate a full system restart. Particularly in environments requiring high reliability, such as safety-critical systems, DUEs can be extremely severe, making their reliability assessment essential [54].

The results of the four fault classifications can be used to obtain the Architectural Vulnerability Factor. The obtained AVF is used as a parameter to calculate the cosmic radiation failure rate (SER_{System}) of the system.

4. Case Study

We conducted case studies and analyses to validate the integrated failure rate analysis proposed in Section 3. Section 4.1 introduces 23 types of hardware circuits utilized for the case studies. Section 4.2 presents the results of the integrated failure rate analysis conducted on these circuits. Section 4.3 confirms the validity of the integrated failure rate model by comparing it with previous studies.

4.1. Test Bench Circuit

In this study, we selected three types of test bench circuits for each circuit category to facilitate the case study. For the combinational circuit, the ISCAS85 benchmark was chosen. The ISCAS85 is a widely used combinational logic circuit benchmark designed for research purposes, comprising a netlist, a Verilog hierarchical structural model, and a hierarchical behavioral model [55]. The ITC99 was selected as the test bench circuit for the sequential circuit category. ITC99 is a series of sequential circuit benchmarks developed by the CAD Group for experimentation with Design for Testability (DFT) and Automatic Test Pattern Generation (ATPG). For the security circuit test benches, AES128, RSA, and SHA were selected. These security circuits are core elements of modern cryptographic security systems, performing various security functions, including encryption, decryption, integrity checking, and authentication.

4.2. Integrated Failure Rate Analysis

For the integrated failure rate analysis, we conducted both atmospheric radiation failure rate estimation and physics-of-failure analysis. To assess cosmic radiation failure rates, we carried out a Statistical Fault Injection (SFI) campaign on the Verilog simulation model of the test bench circuit. The model under SFI testing uses test bench circuits

implemented at the RTL level. To calculate the number of Statistical Fault Injection (SFI) tests, it is essential to first determine the total test space of the target system. This total test space can be computed as the product of two factors: (1) the Verilog objects (such as inputs, outputs, and wires) that are susceptible to defect injection and (2) the time space available for defect injection. In this context, the time space is proportional to the number of test vectors applied to the circuit, which defines the temporal dimension in which faults can be introduced.

Once the total defect space is identified, the required number of tests can be determined using a statistical formula that incorporates the desired confidence interval level. In this study, the number of tests was calculated based on a 95% confidence interval, ensuring statistically reliable results [49]. After performing the SFI tests, the Architectural Vulnerability Factor ($AVF_{circuit}$) for the test bench circuit was calculated. Using the $AVF_{circuit}$, the Soft Error Rate ($SER_{Circuit}$) was then estimated, providing a quantitative assessment of the circuit's susceptibility to atmospheric radiation-induced failures.

For the analysis of physics of failure, the PoF_{System} was determined using a three-step process with Sherlock software: environment and configuration setup, simulation, and PoF analysis.

In the first step, component modeling and the definition of temperature profiles were conducted. To facilitate a comprehensive understanding of the physics of failure (PoF) analysis, we outlined the process performed on a 28 nm MOSFET chip. The component parameters required for modeling this part (e.g., current, voltage, temperature, number of pins, package, etc.) are detailed in Appendix B.

Calculating the four PoFs—Hot Carrier Injection (HCI), Negative Bias Temperature Instability (NBTI), Time-Dependent Dielectric Breakdown (TDDB), and Electromigration (EM)—requires specific parameters. Some of these parameters are obtainable from standard documents such as JEP-122F (JEDEC Engineering Procedure 122F), as shown in Table A1 in Appendix A, or from data sheets such as Appendix B. JEP-122F provides standardized procedures for the reliability evaluation of semiconductor devices and defines the key parameters essential for PoF analysis [44]. However, certain parameters, including acceleration factors and empirical exponents, are proprietary and not publicly available. These non-public parameters represent internal optimization factors related to package design and are critical for enhancing the accuracy of PoF analysis.

To address the absence of these proprietary parameters, this study utilizes Sherlock software, as illustrated in Figure 4. Sherlock software generates proprietary data based on external input conditions (e.g., Package, Die, Electronic, Test, and IC wearout) to perform PoF analysis. Specifically, scaling factors are automatically generated within Sherlock software, enabling reliable PoF analysis through the integration of extensive experimental data and validated models.

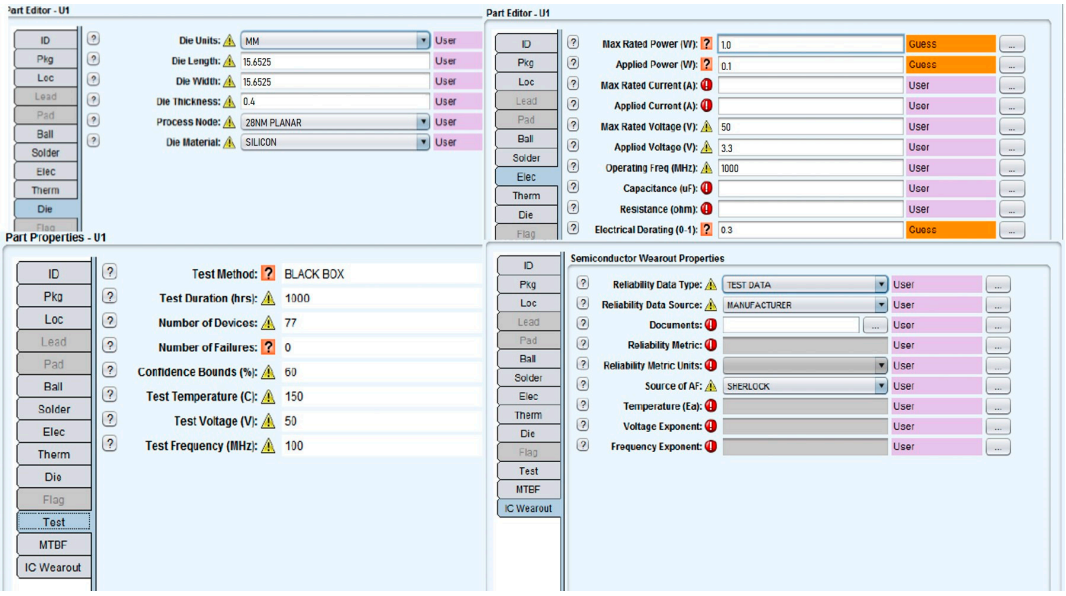

Figure 4. Input parameter interface for semiconductor reliability analysis in Sherlock software.

Temperature profile definition was conducted to accurately replicate the operational environment of the components. These profiles were established in accordance with MIL-STD-810H Part 1 Annex C, a widely recognized military standard for environmental testing procedures [18]. The specific temperature-time profile tables applied in this study are detailed in Appendix C.

In the second step, the previously defined information (component and environmental data) was used to conduct a wear-out analysis of the device. The failure rate models employed were the four failure mechanisms defined in the JEP122F standard: Hot Carrier Injection (HCI), Time-Dependent Dielectric Breakdown (TDDB), Negative Bias Temperature Instability (NBTI), and Electromigration (EM) [44].

The third step, PoF analysis, uses the Sherlock tool to provide time-dependent failure probabilities based on the results of the physics-of-failure analysis for each device. The failure probabilities over time are derived from the failure rates of the four failure models. The failure probability model used was an exponential distribution, which aligns with the modeling approach commonly employed in JEDEC standards. This methodology is well-suited for ensuring reliability during the early development stages.

As a result, the integrated failure rate for 23 test bench circuits was calculated, as shown in Table 2.

Table 2. Results of integrated failure rate (Flux = 2.04×10^3, $PoF_{System} = 1.48 \times 10^{-5}$).

Classification	Circuit	$AVF_{circuit}$	SER_{System}	IFR_{System}
ISCAS85	C432	23.66%	3.46×10^{-6}	1.82×10^{-5}
	C499	38.71%	5.66×10^{-6}	2.04×10^{-5}
	C880	30.32%	4.43×10^{-6}	1.92×10^{-5}
	C1355	22.70%	3.32×10^{-6}	1.81×10^{-5}
	C1908	27.24%	3.98×10^{-6}	1.88×10^{-5}
	C2670	21.11%	3.08×10^{-6}	1.79×10^{-5}
	C3540	13.24%	1.94×10^{-6}	1.67×10^{-5}
	C5351	14.79%	2.16×10^{-6}	1.70×10^{-5}
	C6288	56.11%	8.20×10^{-6}	2.30×10^{-5}
	C7552	25.95%	3.79×10^{-6}	1.86×10^{-5}
ITC99	B01	26.10%	3.81×10^{-6}	1.86×10^{-5}
	B02	18.38%	2.68×10^{-6}	1.75×10^{-5}

	B03	25.69%	3.75×10^{-6}	1.85×10^{-5}
	B04	12.70%	1.86×10^{-6}	1.66×10^{-5}
	B05	2.78%	4.06×10^{-7}	1.52×10^{-5}
	B06	32.00%	4.67×10^{-6}	1.95×10^{-5}
	B07	22.09%	3.23×10^{-6}	1.80×10^{-5}
	B08	10.85%	1.59×10^{-6}	1.64×10^{-5}
	B09	17.20%	2.51×10^{-6}	1.73×10^{-5}
	B10	23.10%	3.37×10^{-6}	1.82×10^{-5}
Security Circuit	AES	29.51%	4.31×10^{-6}	1.91×10^{-5}
	RSA	30.73%	4.49×10^{-6}	1.93×10^{-5}
	SHA	22.15%	3.24×10^{-6}	1.80×10^{-5}
Average		23.79%	3.48×10^{-6}	1.83×10^{-5}

4.3. Integrated Failure Rate Review

This section discusses the implications and validation of the integrated failure rate analysis. Section 4.3.1 describes SER and integrated failure rate analysis according to the Earth's operating environment (latitude, longitude, and altitude). Section 4.3.2 evaluates the validity of the integrated failure rate analysis by comparing the Reliability and Mean Time To Failure (MTTF) values derived from our proposed analysis and existing reliability evaluation analysis with actual field data from avionics equipment.

4.3.1. Integrated Failure Rate Analysis in the Global Operating Environment

The integrated failure rate analysis provides a comprehensive assessment of the internal and external factors affecting the reliability of electronic components in a global operating environment. In this section, we examine the impact of cosmic radiation and the integrated failure rate based on key Earth operating environment parameters: latitude, longitude, and altitude. To this end, 20 major cities were selected based on their latitude, longitude, and altitude, and the soft error rate (SER) and integrated failure rate for each city were analyzed [56]. Information for each city is summarized in Appendix D.

An analysis of the effect of cosmic radiation with respect to latitude confirmed that higher latitudes experience higher levels of cosmic radiation. Figure 5 presents the results of a linear regression analysis of cosmic radiation based on latitude and longitude, derived from estimating cosmic radiation for each of the 20 major cities with altitudes below 300 m above sea level. For the estimation of SER according to latitude, the linear regression resulted in $y = 4e^{-10}x + e^{-8}$ ($R^2 = 0.6406$). Since the coefficient of determination R^2 is greater than 0.6, it can be quantitatively confirmed that the effect of cosmic radiation increases with latitude. On the other hand, for the estimation of SER according to longitude, the linear regression resulted in $y = 2e^{-11}x + 3e^{-8}$ ($R^2 = 0.0905$). With an R^2 value less than 0.1, it indicates that there is no significant linear relationship between cosmic radiation and longitude. These results are consistent with those presented in previous studies [13,20,57].

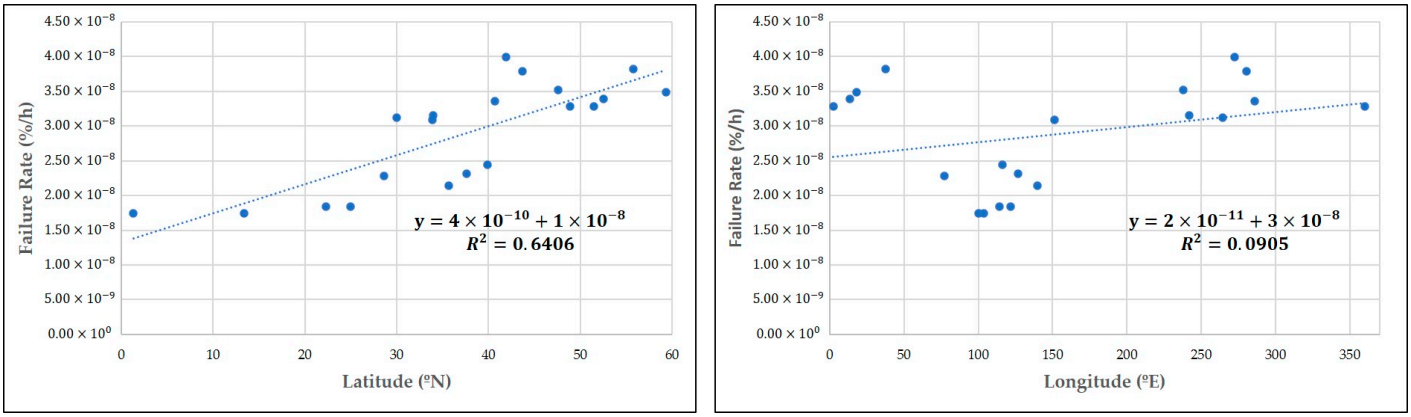

Figure 5. Latitude-based soft error estimation graph (**Left**) and longitude-based soft error estimation graph (**Right**).

The higher the altitude, the greater the impact of the soft error rate (SER) on the reliability of electronic equipment. Figure 6 illustrates the physics of failure rate and the ratio of soft error rates by altitude in eight major cities, as well as in high-altitude regions and aircraft for major commercial FPGA electronic boards [58,59]. At low altitudes (near the Earth's surface), the effect of cosmic radiation on failure rates is minimal, contributing almost less than 2%. However, as the altitude increases, the proportion of cosmic radiation-related failures increases relative to the overall combined failure rate. In particular, when an airplane reaches its operational altitude, the failure rate is estimated to be higher than that predicted by the physics of failure rate analysis alone. This is because the neutron flux approaches its maximum at an altitude of approximately 18.3 km [60].

On the other hand, in the upper atmosphere (above 60–80 km), the atomic density decreases and exceeds the Pfotzer maximum, resulting in a decrease in neutron flux with increasing altitude, while the flux of protons, alpha particles, and heavy ions increases. Below the Pfotzer maximum, more neutrons are removed than are generated, so further decreases in altitude result in lower neutron flux. Consequently, the lower the altitude, the lower the SER, while the higher the operational altitude, the greater the impact of the SER on the reliability of electronic equipment.

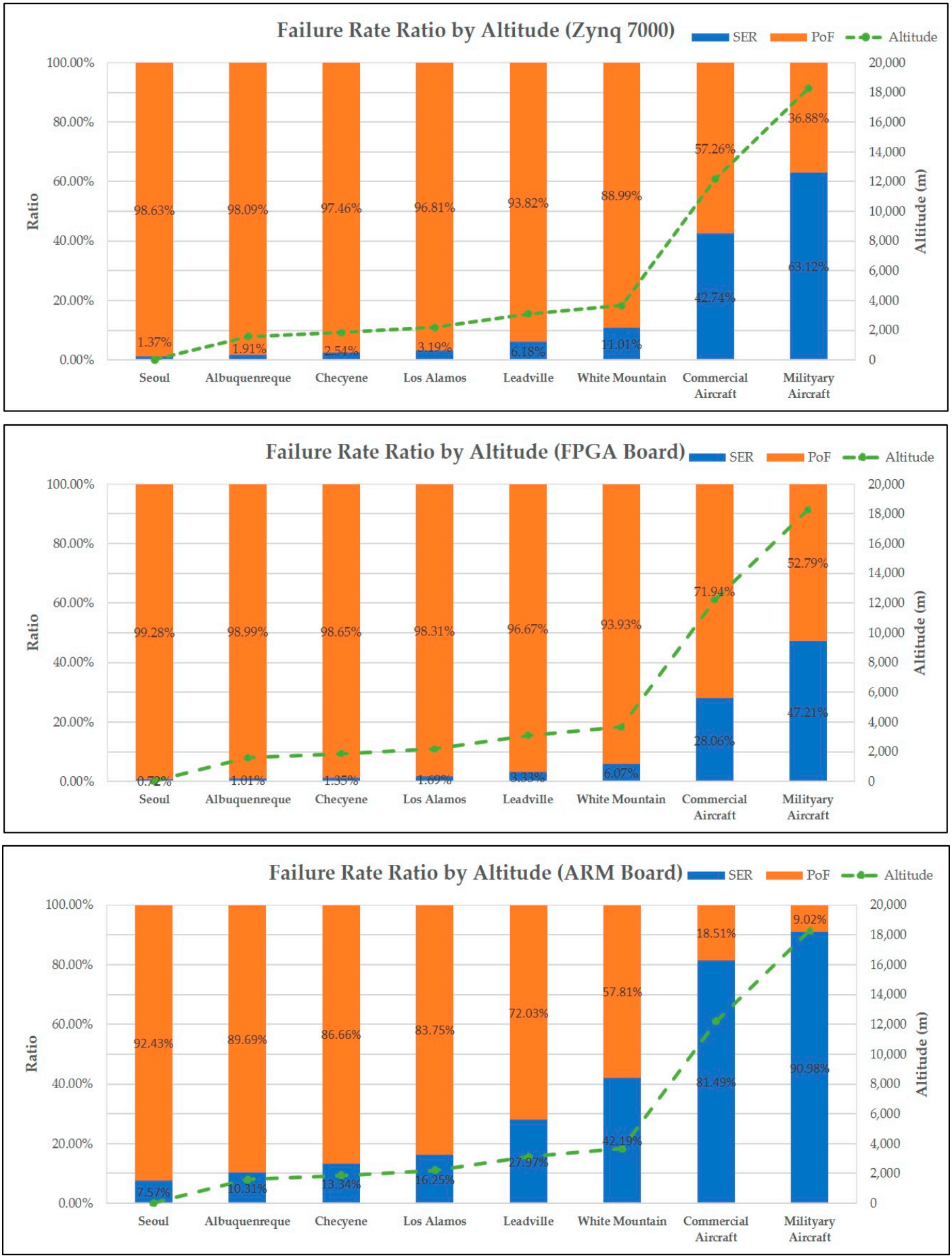

Figure 6. Table of failure rate rates by altitude.

4.3.2. Reliability Assessment of Electronic Equipment Using an Integrated Failure Rate Analysis

In this study, to examine the integrated failure rate analysis, we analyzed the reliability models for electronic equipment boards and the results of the integrated failure rate models. Reliability modeling assumes that the target board is a non-redundant communication board, and an exponential distribution reliability model with a constant failure rate (λ) is applied [61]. Field data were obtained from electronic board data collected by the International Electronics Reliability Institute (IERI) at Loughborough University, UK, and from failure rates of the Circuit Card Assembly in Northrop Grumman's MODAR program (military radar system AN/APN-241) [6,7].

The reliability functions over time, based on various reliability models and field data, are illustrated in Figure 7. The blue lines represent the reliability results from existing models (CNET, HRD4, MIL-HDBK 217, SimCenter) [8,9]. The red lines show the reliability results derived from field data of electronic boards used in military aircraft [6,7]. The purple line indicates the mean value of the integrated failure rate calculated in this study. Additionally, the dashed purple lines represent the 95% confidence interval bounds for the integrated failure rate. The results of the graph provide the following insights:

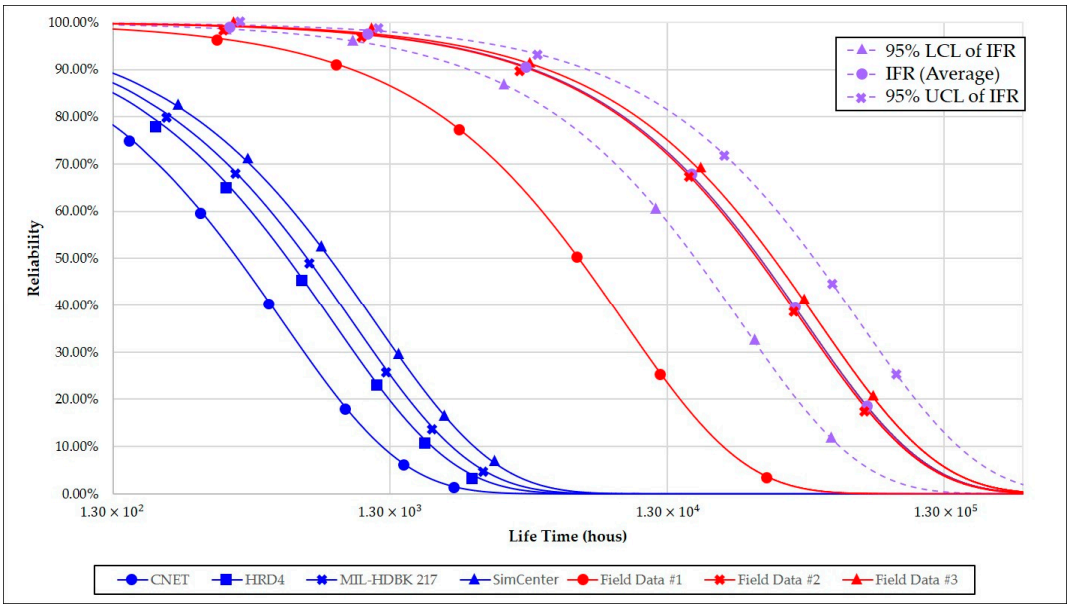

Figure 7. Graph of electronic equipment reliability model comparison results.

First, previous reliability analysis often underestimates the reliability of board components. For example, one study found that the expected failure rate of telecommunications components was lower than the actual field failure rate [9]. Another study showed that the failure rate predicted by the MIL-HDBK-217 model did not match real-world data [6]. These models are conservative, focusing on minimizing unplanned failures and ensuring safety. However, they rely on simplified assumptions that ignore real-world factors, such as usage, environmental conditions, and aging effects. This underestimation leads to unnecessary maintenance, higher costs, and reduced operational efficiency. Premature replacements and over-maintenance can negatively affect system performance and cost-effectiveness.

Second, the analysis of the integrated failure rate model revealed a significant reduction in error compared to the actual failure rate observed in the field. Unlike existing reliability models, the integrated model effectively addresses the issue of underestimating reliability. In this study, the MTTF values were calculated by taking the reciprocal of the failure rate values obtained from Figure 7 at an altitude of 20,000 feet. The resulting MTTF

value for the integrated failure rate model was calculated as the reciprocal of the average failure rate (1.83×10^{-5}), is 5.46×10^{4}. This value is significantly higher than the average MTTF of 8.52×10^{2} derived from existing reliability models. Moreover, it closely aligns with the average field-measured value of 3.14×10^{4}. This improvement stems from the integrated model's ability to incorporate multiple failure mechanisms, including both atmospheric radiation-induced failures and wear-out mechanisms, with more precision. By accurately reflecting these mechanisms under specific environmental conditions, such as the 20,000-foot altitude used as a reference, this model offers a more realistic assessment of failure probabilities in real-world operating environments, providing greater reliability than traditional models.

5. Conclusions

This study introduces an integrated failure rate (IFR) analysis that delivers essential failure rate data for aerospace system safety analysis, as outlined in SAE ARP 4761A [62]. Utilizing the Sum-of-the-Failure-Rates Method from JEDEC JEP122E, the IFR method accurately combines the radiation failure rate and aging failure rate, providing an acceptable failure rate during the early stages of system safety analysis [45]. To address the limitations of previous reliability analysis, the proposed IFR analysis incorporates failure rates caused by atmospheric radiation and aging mechanisms. The physics of failure rate was measured using the Sherlock tool, a physical failure analysis tool, while the atmospheric radiation failure rate was calculated using a semi-empirical Soft Error Rate model. As a case study, the combined failure rate was analyzed for various test circuits based on their location and operating environment, including latitude, longitude, and altitude. Furthermore, the validity of the IFR analysis was confirmed by comparing its estimates with field data from avionics equipment and previous reliability analyses.

Previous reliability analyses tend to underestimate the reliability of board components, leading to inconsistencies with actual failure rates, resulting in increased maintenance costs and reduced operational efficiency. This trend was also confirmed by the studies conducted by various researchers, noting that the estimated failure rate of the MIL-HDBK-217 did not match the field data. The integrated failure rate presented in this study mitigates the limitations of existing models and significantly reduces the error compared to the actual failure rates observed in the field by incorporating the additional failure rate caused by atmospheric radiation. Our results align with the field data, indicating that it can be regarded as a more practical and dependable method for the system safety analysis.

Author Contributions: Data review and visualization were performed by D.L., and paper writing and editing were managed by D.L. and J.N. All authors have read and agreed to the published version of the manuscript.

Funding: This work was partly supported by the GRRC program of Gyeonggi province (GRRC Korea Aerospace University 2023-B02) and the National Research Foundation of Korea (NRF), as well as a grant funded by the Korean government (MSIT) (No. 2022K1A3A1A2001493).

Informed Consent Statement: Not applicable.

Data Availability Statement: The data presented in this study are available upon request from the corresponding author.

Conflicts of Interest: The authors declare no conflicts of interest.

Abbreviations

The following abbreviations are used in this manuscript:

Abbreviation	Full Name	Description
AVF	Architectural Vulnerability Factor	A coefficient representing the extent to which a designed circuit is susceptible to soft errors.
ARP	Aerospace Recommended Practice	A set of guidelines and standards developed for aerospace systems to ensure safety, reliability, and performance.
EM	Electromigration	A failure mechanism caused by the movement of metal atoms due to electron flow.
FPGA	Field Programmable Gate Array	A semiconductor device containing programmable logic blocks and interconnects.
HCI	Hot Carrier Injection	A phenomenon in solid-state devices where electrons or holes gain enough energy to break interface states.
IFR	Integrated Failure Rate	A failure rate model combining physics of failure rate and soft error rate.
JEDEC	Joint Electron Device Engineering Council	An independent semiconductor engineering trade organization that develops open standards for microelectronics and the semiconductor industry.
NBTI	Negative Bias Temperature Instability	Instability in PMOS transistors caused by characteristic changes at high temperatures.
PCR	Primary Cosmic Rays	High-energy particles from outer space, mainly protons, that continually bombard the Earth.
PoF	Physics of Failure	A methodology for analyzing the physical causes of failure mechanisms.
SAE	Society of Automotive Engineers	An international organization that develops standards for the automotive, aerospace, and mobility industries.
SCR	Secondary Cosmic Rays	Secondary cosmic rays, caused by the decay of primary cosmic rays, include photons, hadrons, and leptons.
SEE	Single Event Effect	A variety of error phenomena caused by a single radiation particle, including SEU.
SEU	Single Event Upset	A transient bit flip in memory or flip-flops caused by a radiation particle.
SER	Soft Error Rate	The rate of soft errors caused by radiation.
SET	Single Event Transient	A momentary voltage spike at a node in an integrated circuit caused by a single energetic-particle strike.
SFI	Statistical Fault Injection	A statistical method for evaluating reliability through fault injection.
TDDB	Time-Dependent Dielectric Breakdown	A failure caused by the time-dependent degradation of an oxide layer.
TID	Total Ionizing Dose	The total amount of ionizing energy accumulated in a device due to radiation.

Appendix A

$$PoF_{HCI} = A_{HCI}\left(\frac{I_{sub}}{W}\right)^{m}\exp\left(-\frac{E_{aHCI}}{\kappa T}\right) \tag{A1}$$

$$PoF_{NBTI} = A_{NBTI}V_{gs}^{\frac{1}{\tau}}\left[\frac{1}{1+2\exp\left(-\frac{E_1}{\kappa T}\right)}+\frac{1}{1+2\exp\left(-\frac{E_2}{\kappa T}\right)}\right]^{\frac{1}{\tau}} \tag{A2}$$

$$PoF_{TDDB} = A_{TDDB}A^{\frac{1}{\beta}}V_{gs}^{a+bT}\exp\left(\frac{c}{T}+\frac{d}{T^2}\right) \tag{A3}$$

$$PoF_{EM} = A_{EM}J^{n}\,exp\left(-\frac{E_{aEM}}{\kappa T}\right) \tag{A4}$$

Table A1. Physics of failure parameters of 28nm MOSFET Chip [44].

Parameter	Function or Purpose	Unit	Data
A_{EM}	Accelerator Factor of EM		Not Disclosed
J	Current Density	A/m	2242.42
n	Exponent of EM		2
E_{aEM}	Activation energy of EM	eV	0.9
κ	Boltzmann's constant	eV/K	8.617×10^{-5}
T	Temperature	K	300
A_{HCI}	Accelerator Factor of HCI		Not Disclosed

I_{sub}	Sub Threshold Current	A	1.48×10^{-3}
m	Exponent of HCI		Not Disclosed
W	Channel Region Width	M	3.00×10^{-7}
E_{aHCI}	Activation energy of HCI	eV	−0.15
A_{TDDB}	Accelerator Factor of TDDB		Not Disclosed
β	Weibull Beta TDDB		1
V_{gs}	Nominal Core Voltage	V	0.8
a, b	Voltage Dependence Coefficient		Not Disclosed
c, d	Temperature Dependence Coefficient		Not Disclosed
A_{NBTI}	Accelerator Factor of NBTI		Not Disclosed
E_1, E_2	Activation energy of NBTI	eV	0.6
τ	Exponent of TDDB		Not Disclosed

Appendix B

Table A2. Product specification summary.

Item	Details
Pin (I/O)	Quantity: 125 pcs Allowed Voltage: 1.2~3.3 V
Pin (Peripheral)	Quantity: 128 pcs
Size	Dimensions: 17 × 17 nm/Ball Pitch: 0.8 mm
Power (Current)	Absolute Max: 12 mA Recommended: 10 mA
Power (Voltage)	Absolute Max: 0.5~1.1 V Recommended: 0.95~1.00 V
Temperature (Commercial)	0~85 °C
Temperature (Industrial)	−40~100 °C

Appendix C

Table A3. Temperature profile table (Republic of Korea).

State	Season (Daily Cycle)	Temperature			Hours (1 yrs)	Life		Profile (Hours)				Count (24 h)
		Duration (Month)	Daily Low	Daily High		Design (10 yrs)	%	Min Temp	Ramp Up	Max Temp	Ramp Down	
On Duty (30%)	Spring/Fall (A3)	6	28	39	1296	12,960	15.0	6	6	6	6	540
	Summer (B2)	3	26	35	648	6480	7.5	6	6	6	6	270
	Winter (C1)	3	−32	−21	648	6480	7.5	6	6	6	6	270
	Sub Total	12	-	-	2592	25,920	30.0			-		1080
Off Duty (70%)	Spring/Fall (A3)	6	28	58	3024	30,240	35.0	6	6	6	6	1260
	Summer (B2)	3	30	63	1512	15,120	17.5	6	6	6		630
	Winter (C1)	3	−33	−25	1512	15,120	17.5	6	6	6	6	630
	Sub Total	12	-	-	6048	60,480	70.0			-		2520
	Total				8640	86,400	100.0			-		3600

Appendix D

Table A4. Location information by major city and flux table.

City	Nation	Latitude (ºN)	Longitude (ºE)	Elevation (m)	Relative Neutron Flux
Bangkok	Thailand	13.4	100.3	20	0.52
Beijing	China	39.9	116.4	55	0.73
Beriln	Germany	52.5	13.4	40	1.01
Denver	USA	41.9	272.4	180	1.19
Hongkon	China	22.3	114.2	30	0.55
Houston	USA	30.0	264.6	15	0.93
London	UK	51.5	359.9	10	0.98
Los Angeles	USA	34.0	241.7	100	0.94
Moscow	Russia	55.8	37.6	150	1.14
New Delhi	India	28.6	77.2	220	0.68
New York	USA	40.7	286	0	1
Paris	France	48.9	2.3	50	0.98
Settle	USA	47.6	237.7	50	1.05
Seoul	South Korea	37.6	127	50	0.69
Sidney	Australia	–33.9	151.2	30	0.92
Singapore City	Singapore	1.3	103.9	15	0.52
Stockholm	Sweden	59.3	18.1	30	1.04
Taipei	Taiwan	25.0	121.5	10	0.55
Toronto	Canada	43.7	280.6	120	1.13

References

1. Chatterjee, I.; Narasimham, B.; Mahatme, N.N.; Bhuva, B.L.; Reed, R.A.; Schrimpf, R.D.; Wang, J.K.; Vedula, N.; Bartz, B.; Monzel, C. Impact of technology scaling on SRAM soft error rates. *IEEE Trans. Nucl. Sci.* **2014**, *61*, 3512–3518.
2. Dodd, P.; Shaneyfelt, M.; Felix, J.; Schwank, J. Production and propagation of single-event transients in high-speed digital logic ICs. *IEEE Trans. Nucl. Sci.* **2004**, *51*, 3278–3284.
3. National Aeronautics and Space Administration. Space Math III Problem 6: Single Event Upsets in Aircraft Avionics. Available online: https://www.nasa.gov/sites/default/files/files/SMIII_Problem6.pdf (accessed on 14 September 2024).
4. Certification Memorandum Single Event Effects (SEE) Caused by Atmospheric Radiation EASA CM No.: CM-AS-004 Issue 01, January 2018. Available online: https://www.easa.europa.eu/sites/default/files/dfu/CM-AS-004%20Issue%2001.pdf (accessed on 14 September 2024).
5. Damkjar, S.E.; Mann, I.R.; Elliott, D.G. Proton beam testing of SEU sensitivity of M430FR5989SRGCREP, EFM32GG11B820F2048, AT32UC3C0512C, and m2s010 microcontrollers in low-earth orbit. In Proceedings of the 2020 IEEE Radiation Effects Data Workshop (in Conjunction with 2020 NSREC), Virtual, 30 November–30 December 2020; IEEE: New York, NY, USA, 2020; pp. 1–5.
6. Brown, L.M. Comparing reliability predictions to field data for plastic parts in a military, airborne environment. In Proceedings of the Annual Reliability and Maintainability Symposium, Tampa, FL, USA, 27–30 January 2003; IEEE: New York, NY, USA, 2003; pp. 207–213.
7. Nalos, E.J.; Schulz, R.B. Reliability and cost of avionics. *IEEE Trans. Reliab.* **1965**, *14*, 120–130.
8. Denson, W. *Handbook of 217Plus Reliability Prediction Models*; RIAC: Moscow, Russia, 2006; p. 146.
9. Jones, J.; Hayes, J. A comparison of electronic-reliability prediction models. *IEEE Trans. Reliab.* **1999**, *48*, 127–134.
10. Pandian, G.P.; DAS, D.; Li, C.; Zio, E.; Pecht, M. A critique of reliability prediction techniques for avionics applications. *Chin. J. Aeronaut.* **2018**, *31*, 10–20.
11. White, M. *Microelectronics Reliability: Physics-of-Failure Based Modeling and Lifetime Evaluation*; Jet Propulsion Laboratory, National Aeronautics and Space Administration: Pasadena, CA, USA, 2008.

12. Bechtold, L.E.; Redman, D. *Integrated Reliability-Roadmap, Framework, and Implementation*; U.S. Department of Transportation Federal Aviation Administration: Washington, DC, USA, 2016.
13. Bolinder, R. Atmospheric Radiation Effects Study on Avionics: An Analysis of NFF Errors. Masters's Thesis, Linköping University, Linköping, Sweden, 2013.
14. Smith, J.; Doe, A. Design of a tolerant flight control system in response to multiple actuator control signal faults induced by cosmic rays. Aerospace Eng. 2023, 50, 123–135.
15. Lee, B.; Kim, C. Multiple cell upsets inside aircraft: New fault-tolerant architecture. Microelectron. Reliab. 2022, 98, 45–58.
16. Garcia, P.; Wang, T. A detailed methodology to compute soft error rates in advanced technologies. Microprocess. Microsyst. 2024, 105, 105021.
17. Heijmen, T. Analytical semi-empirical model for SER sensitivity estimation of deep-submicron CMOS circuits. In Proceedings of the 11th IEEE International On-Line Testing Symposium, Saint Raphael, France, 6–8 July 2005; IEEE: New York, NY, USA, 2005; pp. 3–8.
18. *MIL-STD-810H*; Department of Defense Test Method Standard for Environmental Engineering Considerations and Laboratory Tests. Department of Defense: Washington, DC, USA, 2019.
19. Lee, D.; Nam, T.; Park, D.; Kim, Y.; Na, J. Enhanced Soft Error Rate Estimation Technique for Aerospace Electronics Safety Design via Emulation Fault Injection. *Appl. Sci.* **2024**, *14*, 1470.
20. Los Alamos National Laboratory. Cosmic Rays; University of California, 3 April 2002. Available online: http://www.lanl.gov/milagro/cosmicrays.shtml (accessed on 2 December 2024).
21. Chavez, J.C.; Hiemstra, D.; Cundar, A.N.; Johnson, B.; Baik, D.; Chen, L. Total Ionizing Dose and Single-Event Effect Response of the AD524CDZ Instrumentation Amplifier. *Energies* **2024**, *17*, 4725.
22. Yin, Y.; Ma, H.; Zheng, Q.; Chen, J.; Duan, X.; Zhang, P.; Zhou, X. Total ionizing dose and single event effect response of 22 nm ultra-thin body and buried oxide fully depleted silicon-on-insulator technology. *Microelectron. Reliab.* **2024**, *152*, 115296.
23. Godlewski, C.; Pouget, V.; Lewis, D.; Lisart, M. Electrical modeling of the effect of beam profile for pulsed laser fault injection. *Microelectron. Reliab.* **2009**, *49*, 1143–1147.
24. Buckley, L.; Dunne, A.; Furano, G.; Tali, M. Radiation test and in orbit performance of mpsoc ai accelerator. In Proceedings of the 2022 IEEE Aerospace Conference (AERO), Big Sky, MT, USA, 5–12 March 2022; IEEE: New York, NY, USA, 2022; pp. 1–9.
25. Casey, M.C.; Goodwill, J.S.; Wyrwas, E.J.; Austin, R.A.; Wilson, C.M.; Stansberry, S.D.; Gorius, N.; Aslam, S. Single-event effects on commercial-off-the-shelf edge-processing artificial intelligence asics. *IEEE Trans. Nucl. Sci.* **2023**, *70*, 1716–1723.
26. Junior, R.L.R.; Malde, S.; Cazzaniga, C.; Kastriotou, M.; Letiche, M.; Frost, C.; Rech, P. High energy and thermal neutron sensitivity of google tensor processing units. *IEEE Trans. Nucl. Sci.* **2022**, *69*, 567–575.
27. Pena-Fernandez, M.; Lindoso, A.; Entrena, L.; Lopes, I.; Pouget, V. Microprocessor error diagnosis by trace monitoring under laser testing. *IEEE Trans. Nucl. Sci.* **2021**, *68*, 1651–1659.
28. Ikemoto, R.; Fujii, S.; Naruse, K.; Shiomi, J.; Midoh, Y.; Yamashita, Y.; Taguchi, M.; Miki, T.; Nagata, M.; Komano, Y.; et al. Double-Sided Multimodal Attack Sensing and Partial Re-Keying in Shared Group Key System. In Proceedings of the 2024 IEEE European Solid-State Electronics Research Conference (ESSERC), Bruges, Belgium, 9–12 September 2024; IEEE: New York, NY, USA, 2024; pp. 681–684.
29. Chen, L.; Ebrahimi, M.; Tahoori, M.B. CEP: Correlated error propagation for hierarchical soft error analysis. *J. Electron. Test.* **2013**, *29*, 143–158.
30. Krishnaswamy, S.; Viamontes, G.F.; Markov, I.L.; Hayes, J.P. Accurate reliability evaluation and enhancement via probabilistic transfer matrices. In Proceedings of the IEEE/ACM International Conference on Design, Automation and Test in Europe (DATE), Munich, Germany, 1–7 March 2005; pp. 282–287.
31. Georgakidis, C.; Valiantzas, D.; Simoglou, S.; Lilitsis, I.; Chatzivangelis, N.; Golfos, I.; Andjelkovic, M.; Sotiriou, C.; Krstic, M. Towards a Comprehensive SET Analysis Flow for VLSI Circuits using Static Timing Analysis. In Proceedings of the 2023 IEEE International Symposium on Defect and Fault Tolerance in VLSI and Nanotechnology Systems (DFT), Juan-Les-Pins, France, 3–5 October 2023; IEEE: New York, NY, USA, 2023; pp. 1–6.
32. Goudet, E.; Treviño, L.P.; Naviner, L.; Daveau, J.-M.; Roche, P. analysis of combinatorial netlists correctness rate based on binomial law and partitioning. In Proceedings of the 2023 IEEE 24th Latin American Test Symposium (LATS), Veracruz, Mexico, 21–24 March 2023; IEEE: New York, NY, USA, 2023; pp. 1–6.
33. Shazli, S.Z.; Tahoori, M.B. Using boolean satisfiability for computing soft error rates in early design stages, Microelectron. *Reliab.* **2010**, *50*, 149–159.

34. Tosaka, Y.; Satoh, S.; Oka, H. An accurate and comprehensive soft error simulator NISES II. In *Simulation of Semiconductor Processes and Devices*; Springer: Vienna, Austria, 2004; pp. 219–222.
35. León, D.; Fabero, J.C.; Clemente, J.A. Non-intrusive study on FPGA of the SEU sensitivity on the COTS RISC-V VeeR EH1 soft processor from Western Digital. *Microprocess. Microsyst.* **2024**, *105*, 105021.
36. Wrobel, F.; Aguiar, Y.; Marques, C.; Lerner, G.; Alía, R.G.; Saigné, F.; Boch, J. An analytical approach to calculate soft error rate induced by atmospheric neutrons. *Electronics* **2022**, *12*, 104.
37. IEEE Reliability Society. *IEEE Standard Framework for Reliability Prediction of Hardware: Revision of IEEE Std 1413–1998*; IEEE Reliability Society: Piscataway, NJ, USA, 2010.
38. Gaonkar, A.; Patil, R.B.; Kyeong, S.; Das, D.; Pecht, M.G. An assessment of validity of the bathtub model hazard rate trends in electronics. *IEEE Access* **2021**, *9*, 10282–10290.
39. Pecht, M.; Kang, W.-C. A critique of MIL-HDBK-217E reliability prediction methods. *IEEE Trans. Reliab.* **1988**, *37*, 453–457.
40. Klutke, G.-A.; Kiessler, P.C.; Wortman, M.A. A critical look at the bathtub curve. *IEEE Trans. Reliab.* **2003**, *52*, 125–129.
41. Gaonkar, A.; Patil, R.B.; Das, D.; Azarian, M.H.; Sood, B.; Pecht, M.G. Assessment of the FIDES Guide 2022 electrical, electronic, and electromechanical reliability prediction methodology. *e-Prime-Adv. Electr. Eng. Electron. Energy* **2023**, *6*, 100353.
42. Lindsey, N.J. NASA Methodology for Physics of Failure-Based Reliability Assessments Handbook; NASA: Washington, DC, USA, 2024.
43. Bechtold, L.E. Industry consensus approach to physics of failure in reliability prediction. In Proceedings of the IEEE Reliability and Maintainability Symposium, San Jose, CA, USA, 25–28 January 2010; pp. 1–4.
44. JEDEC. *Failure Mechanisms and Models for Semiconductor Devices*; Specification JEP-122F; JEDEC: Arlington, VA, USA, 2011.
45. JEDEC. Sum-of-the-Failure-Rates Method. Available online: https://www.jedec.org/standards-documents/dictionary/terms/sum-failure-rates-method (accessed on 2 September 2024).
46. Koren, I.; Krishna, C.M. *Fault-Tolerant Systems*; Morgan Kaufmann: Cambridge, MA, USA, 2020; pp. l1–228.
47. Lauenstein, J.M. Standards for Radiation Effects Testing: Ensuring Scientific Rigor in the Face of Budget Realities and Modern Device Challenges. NASA Technical Report, 21 April 2015. Available online: https://ntrs.nasa.gov/citations/20150011462 (accessed on 17 December 2024).
48. Lee, D.-W.; Na, J.-W. Study of the monte–carlo fault injection simulator to measure a fault derating. *IET Comput. Digit. Tech.* **2019**, *13*, 218–223.
49. Leveugle, R.; Calvez, A.; Maistri, P.; Vanhauwaert, P. Statistical fault injection: Quantified error and confidence. In Proceedings of the 2009 Design, Automation & Test in Europe Conference & Exhibition, Nice, France, 20–24 April 2009; IEEE: New York, NY, USA, 2009; pp. 502–506.
50. SEUTest.com. SEUTest. Available online: http://seutest.com/ (accessed on 9 July 2024).
51. Hiemstra, D.M.; Kirischian, V.; Brelski, J. Single event upset characterization of the Zynq UltraScale+ MPSoC using proton irradiation. In Proceedings of the 2017 IEEE Radiation Effects Data Workshop (REDW), New Orleans, LA, USA, 17–21 July 2017; IEEE: New York, NY, USA, 2017; pp. 1–4.
52. Kelly, A.T.; Rodgers, J.C.; Johnson, S.; Brown, R.D.; Adamson, A. Single Event Effects Characterization of BAE Systems RAD-NET™ 1848-PS RapidIO® Packet Switch. In Proceedings of the 2017 IEEE Radiation Effects Data Workshop (REDW), New Orleans, LA, USA, 17–21 July 2017; IEEE: New York, NY, USA, 2017; pp. 1–6.
53. IEEE Computer Society. IEEE Standard for Verilog Hardware Description Language; IEEE Std 1364-2001; IEEE: Piscataway, NJ, USA, 2001. Available online: https://doi.org/10.1109/IEEESTD.2001.93345.
54. Rech, P. Artificial neural networks for space and safety-critical applications: Reliability issues and potential solutions. In *IEEE Transactions on Nuclear Science*; IEEE: New York, NY, USA, 2024.
55. Brglez, F.; Fujiwara, H. A Neutral Netlist of 10 Combinational Benchmark Circuits and a Target Translator in Fortran; North Carolina State University: Raleigh, NC, USA, 1985.
56. JDEC STANDARD. *Measurement and Reporting of Alpha Particles and Terrestrial Cosmic Ray-Induced Soft Errors in Semiconductor Devices JESD89A*; JEDEC Solid State Technology Association: Arlington, TX, USA, 2006.
57. Normand, E. Single-event effects in avionics. *IEEE Trans. Nucl. Sci.* **1996**, *43*, 461–474.
58. Jiao, J.; De, X.; Chen, Z.; Zhao, T. Integrated circuit failure analysis and reliability prediction based on physics of failure. *Eng. Fail. Anal.* **2019**, *104*, 714–726.
59. Chen, C.; Zeng, Z.-Y.; Jiang, J.-Y.; Ma, X.-L. Correction method of testability verification test plan for electronic product based on physics of failure. In Proceedings of the 2016 Prognostics and System Health Management Conference (PHM-Chengdu), Chengdu, China, 19–21 October 2016; IEEE: New York, NY, USA, 2016; pp. 1–6.

60. NASA. Cosmic Rays—Introduction. 3 February 2010. Available online: http://imagine.gsfc.nasa.gov/docs/science/know_l1/cosmic_rays.html (accessed on 20 October 2024).
61. Benevenuti, F.; Kastensmidt, F.L. Comparing exhaustive and random fault injection methods for configuration memory on SRAM-based FPGAs. In Proceedings of the 2019 IEEE Latin American Test Symposium (LATS), Santiago, Chile, 11–13 March 2019; IEEE: New York, NY, USA, 2019; pp. 1–6.
62. ARP4761 S.A.E. Guidelines and Methods for Conducting the Safety Assessment Process on Airborne Systems and Equipments; The Engineering Society for Advancing Mobility Land Sea Air and Space: Warrendale, PA, USA, 1996.